

PCCP

Influence of 1-methyl-3-octylimidazolium chloride on MIL-53(Al) crystallinity and particle size

Journal:	Physical Chemistry Chemical Physics
Manuscript ID	CP-COM-07-2024-002981.R2
Article Type:	Communication
Date Submitted by the Author:	24-Oct-2024
Complete List of Authors:	Wang, Oliver; Bowdoin College, Department of Chemistry Vadlamudi, Pranav; Bowdoin College, Department of Chemistry Jang, Victoria; Bowdoin College, Department of Chemistry Hoadley, Andrew; Bowdoin College, Department of Chemistry Ortoll-Bloch, Amnon G.; Bowdoin College, Department of Chemistry

SCHOLARONE™ Manuscripts

COMMUNICATION

Influence of 1-methyl-3-octylimidazolium chloride on MIL-53(Al) crystallinity and particle size

Received XXX Accepted XXX Oliver Wang, ^a Pranav Sai Vadlamudi, ^a Victoria Jang, ^a Andrew Hoadley, ^a and Amnon G. Ortoll-Bloch*, ^a

DOI: XXX

- ^a Department of Chemistry, Bowdoin College, Brunswick, ME 04011, USA
- *Corresponding author can be contacted at: a.ortollbloch@bowdoin.edu

Little is known about ionic liquids as MOF crystallization additives. We investigate the role of 1-methyl-3-octylimidazolium chloride (OmimCl) in MIL-53(Al) hydrothermal synthesis. Higher crystallinities and particle sizes with 0.05% – 0.50% v/v OmimCl suggest preferential growth along [001]. With 1.0% – 10% v/v OmimCl, missing linkers and lower crystallinities indicate arrested growth.

Metal-organic frameworks (MOFs) are porous, crystalline solids consisting of metal oxide clusters cross-linked by organic linkers.¹ MIL-53(AI), consisting of AIO₄(OH)₂ chains cross-linked by 1,4benzenedicarboxylate (BDC) ligands, is a MOF that exhibits high thermal stability, flexible porosity, excellent moisture resistance, and high internal surface area.^{2,3} These properties make MIL-53(Al) attractive for efficient gas storage,4 as well as the adsorption and photocatalytic degradation of dyes and pharmaceuticals for wastewater treatment.⁵ However, much is still unknown about how MIL-53(AI) crystallizes from solution in the presence of additives. Crystallization additives, even when used in low concentrations, can bind to crystal surfaces and precursor ions, influencing the crystallization pathway.⁶⁻⁸ Common additives in MOF synthesis include acetic acid, which acts as a modulator that caps growth complexes and grows larger particles, and bases such as triethylamine and NaOH, which increase the pH to promote faster nucleation and smaller particle sizes.9-11 Ligands used during MOF synthesis can also guide the crystallization process. As an example, 2-methylimidazole acts as both the linker and morphologycontrolling additive in the synthesis of ZIF-8.12 High 2methylimidazole-to-metal ratios resulted in rhombic dodecahedron morphologies and smaller crystal sizes, while lower ratios resulted in a cubic morphology and larger crystal sizes. Crystal size and morphology control can also be achieved using surfactants, which can either interact with different crystal facets to accelerate growth in specific directions or coalesce to introduce hierarchal pores that give rise to new morphologies. 13-15 Molina et al. demonstrated that NH₂-MIL-53(Al) growth with cetrimonium bromide (CTABr) resulted in a significant incorporation of surfactant into the MOF when CTABr/Al molar ratios of 0.6 or above were used. 16 Micelle formation

of CTABr introduced hierarchical pores in NH₂-MIL-53(AI), which was reflected by new X-ray diffraction (XRD) peaks. Similarly, Habib *et al.* demonstrated that using non-ionic surfactants Pluronic F127 and P123 for NH₂-MIL-53(AI) crystal growth increased the XRD peak intensities for certain peaks, suggesting that Pluronic F127 aligned individual MOF crystallites to promote preferential growth along a specific direction, resulting in long, rod-shaped crystals.¹⁷ These results suggest that additives exert significant influence on the crystallization pathways of MOFs. Investigating the growth of MIL-53-type MOFs in the presence of additives will contribute to a deeper understanding of the role of additives in MOF crystallization, which, in turn, will help achieve higher synthetic control.

Ionic liquids (ILs) are a class of organic salts that have been a leading solvent choice for MOF synthesis, due to their negligible vapor pressure and tunable structure.18 MOF synthesis using ILassisted methods typically demonstrates increased MOF crystallinity, significantly shortened synthesis times, and the ability to recover the synthesis solution for repeated, high-quality synthesis. 19,20 One of the more commonly used ILs for MOF synthesis is 1-methyl-3octylimidazolium chloride (OmimCl), which will be the focus of this study.^{20–22} When utilized as a solvent for the synthesis of UiO-66, OmimCl significantly accelerated the rate of crystallization of UiO-66 at room temperature compared to conventional organic solvents such as dimethylformamide, shortening the synthesis time from 120 h to 50 min.²⁰ OmimCl promotes the coordination between linkers and the pre-MOF cluster, leading to rapid crystallization at room temperature. A recent review included over 60 examples where ILs were used as solvents.19 Novel MOFs of varying composition and topology were generated via IL cation templating into the MOF crystal lattice and occasional incorporation of the halide counter anion of the IL.^{23–25} While there are examples of MOFs synthesized in ILs via ionothermal synthesis, there is insufficient research on using ILs as additives (not solvents) in MOF crystallization.¹⁹ Hence, this work focuses on elucidating the effects of the IL OmimCl on MIL-53(Al) crystallization by carrying out hydrothermal syntheses using varying amounts of OmimCl as the additive. Comparisons amongst samples are made by examining crystallinity with XRD, the crystal morphology, size, and assembly

COMMUNICATION PCCP

using scanning electron microscopy (SEM), and the composition using ¹H nuclear magnetic resonance (NMR) digestion analysis. Our findings help inform on how ILs affect MOF crystallization as additives and contribute toward predictive MOF synthesis.

MIL-53(Al) was synthesized using Al(NO₃)₃·9H₂O and 1,4-benzenedicarboxylic acid (BDC) as precursors under the hydrothermal method inside a sealed Parr vessel at 200 °C for 24 h. After calcination, XRD showed a phase-pure narrow-pore (np) phase. From XRD peak width analysis, the average crystallite size from the three most intense peaks (*i.e.*, the (200), (110), and (11 $\overline{1}$) reflections) was calculated as 34.4 \pm 1.8 nm (Fig. 1, black trace). This crystallite size value is similar to that obtained by Taheri *et al.* (42.6 nm) under similar synthesis conditions. 26 ATR-FTIR spectroscopy confirmed that all free BDC linker had been removed by calcination as indicated by the absence of a peak around 1700 cm $^{-1}$ (Fig. S1), which is attributed to the carboxylate group of the free BDC linker. All other IR vibrations correspond with literature values. 27

To understand the effect of OmimCl concentration on the hydrothermal synthesis of MIL-53(Al), eight samples were synthesized: one pure MIL-53(AI)-np sample without the addition of OmimCl (sample 1) and samples where 0.05% (sample 2), 0.10% (sample 3), 0.20% (sample 4), 0.50% (sample 5), 1.0% (sample 6), 5.0% (sample 7), and 10% (sample 8) v/v OmimCl was added to the initial synthesis solution. XRD indicates that certain crystallographic reflections increase in intensity with increasing OmimCl concentrations up to 0.50% v/v, most notably the (110), (020), (220), (130), (620), and (800) reflections at 12.4°, 23.2°, 25.8°, 35.5°, 36.9°, and 37.8°, respectively (Fig. 1a,b). Defining the relative crystallinity against the sample with the highest XRD peak intensity (sample 5, synthesized with 0.50% v/v of OmimCl), the results indicate up to a 43% improvement in relative crystallinity from sample 1 to sample 5 (Fig. 1d). The increasing intensity of {hk0} reflections suggests that the preferential growth of {hk0} faces is promoted in the presence of up to 0.50% v/v OmimCl, which leads to elongation of the crystal along the [001] direction. 28,29 Since the MIL-53(Al) crystal has its length and pore aligned along the c-axis,²⁹ it can be deduced that OmimCl promotes both overall crystallinity and preferential growth along the [001] direction. For samples 1 through 5, the crystallite sizes are in agreement within uncertainty (Table S1). However, this observation is only supported up to 0.50% v/v IL. At higher concentrations, the relative crystallinity decreased from the maximum (sample 5) to 0.20 for sample 8 (Fig. 1d). Curiously, the crystallite size at concentrations above 0.50% v/v OmimCl increases from 35.5 \pm 1.5 nm (sample **5**) to 39.3 \pm 2.2 nm (sample **8**). An explanation towards this discrepancy is yet to be determined.

OmimCl concentrations above 0.50% v/v introduced defects into the MOF crystals. NMR digestion analysis indicates that the linker weight decreased from 72.2 – 74.2% at IL volume fractions below 0.50% (expected: 72.6%) to 43.4 – 67.8% at IL volume fractions of 1.0 – 10% (Table S2). Accordingly, the XRD patterns of samples 7 and 8 show several broad peaks (14.5°, 27.2°, 38.2°) that correspond with the XRD reflections of boehmite (γ -AlO(OH)), which is formed when undercoordinated Al sites are oxidized during the calcination process (Fig. 1c).³⁰ Notably, these boehmite XRD reflections are completely

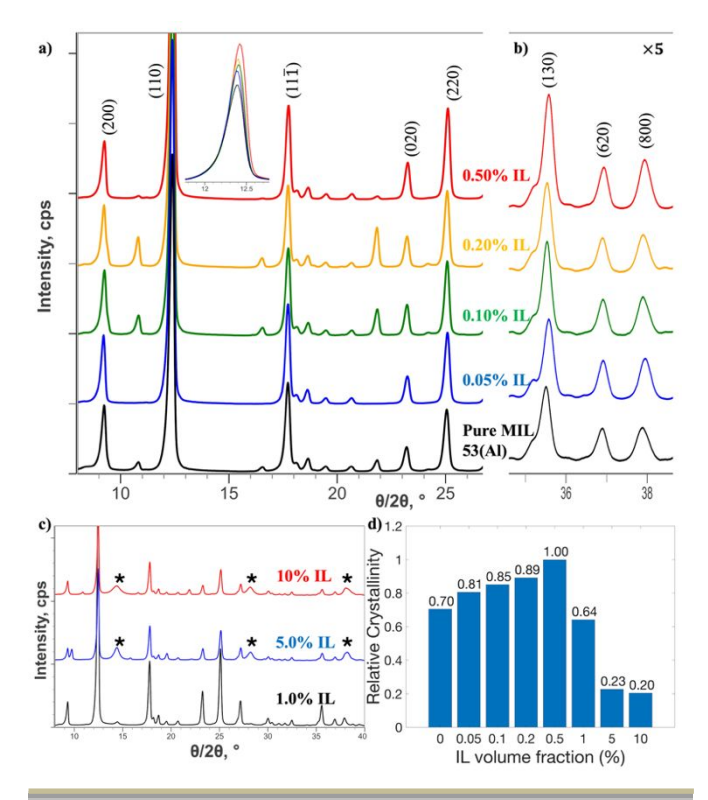


Figure 1. a) XRD patterns of pure MIL-53(Al)-np (black) and MIL-53(Al) synthesized with 0.05% (blue), 0.10% (green), 0.20% (orange), and 0.50% (red) v/v OmimCl. Expanded views for the (110) peak (inset) and the (130), (620), and (800) peaks (b) are shown. c) XRD patterns of MIL-53(Al) synthesized with 1.0% (black), 5.0% (blue), 10% (red) v/v OmimCl. Markers (*) indicate characteristic peak locations for boehmite. d) Relative crystallinities for MIL-53(Al) synthesized in the presence of various IL volume fractions.

absent in samples **1** - **5**. These observations suggest that IL concentrations above 0.50% v/v led to the formation of defects. The extent of defect formation needs to be investigated with thermogravimetric analysis (TGA) and elemental analysis and will be the subject of future work.

SEM particle size measurements provide further evidence of preferential growth. Pure MIL-53(AI)-np is characterized by a mixture of small block-like and needle-like crystals (Fig. 2a). As more OmimCI was dissolved in the initial synthesis mixture, the particle size increased from $4.9\pm1.2~\mu m$ in sample 1 to $7.8\pm2.3~\mu m$ in sample 5, with the crystals becoming larger and more block-like for samples 4 and 5 (Fig. 2b,c). The absence of needle-like crystals in the presence of OmimCI suggests that OmimCI inhibits the formation of needle-like crystal morphologies. Some particles appear to be polycrystalline assemblies, as evidenced by fracture lines parallel to the length of the crystals or by crystals growing out of each other (Fig. 2c, d). Samples 6, 7, and 8 show large crystal aggregates of up to 40 μ m wide as well as irregularly shaped particles (Fig. 2e), with the average particle size decreasing to 6.3 - 6.7 μ m (Fig. 2f). SEM images for samples 2, 3, and 7 are provided in Figures S2-S4.

SEM results are, therefore, in agreement with XRD results, indicating preferential growth along the length of the crystal in the presence of up to 0.50% v/v OmimCl. Both SEM and XRD measurements follow the same trend, where maximum particle size

PCCP

COMMUNICATION

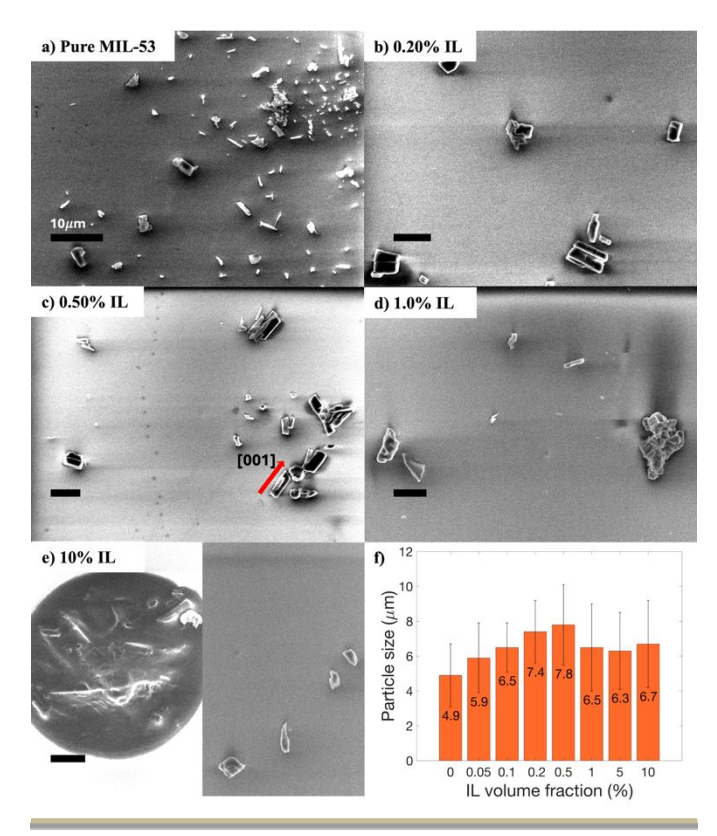


Figure 2. SEM images of: a) Pure MIL-53(Al)-np crystals (1), and crystals grown with the addition of: b) 0.20% v/v IL (4); c) 0.50% v/v IL (5); d) 1.0% v/v IL (6); e) 10% v/v IL (8). The c-axis, or the [001] direction, is highlighted for one crystal in c) by an adjacent red arrow. f) Particle sizes measured by SEM for all samples.

and relative crystallinity are observed when 0.50% v/v IL was dissolved into the initial synthesis solution. The increase in particle size and relative crystallinity represents a significant improvement from pure MIL-53(Al). At IL concentrations above 0.50% v/v, both particle size and relative crystallinity decrease, with the presence of large crystal agglomerates and irregularly shaped particles (Figs. 1d and 2f). The largest crystal size obtained in this work surpassed that of MIL-53(AI) synthesized under conventional hydrothermal conditions (220 °C, 3 days, average particle size: 3.6 µm),¹⁷ showing that IL addition is a promising method to obtain larger crystals of MIL-53(AI) using less time and energy. Since higher crystallinity usually corresponds to higher stability and better physical properties for MOF crystals, these results contribute towards the synthesis of highquality MOF crystals suitable for their intended applications.^{26,27} In contrast, crystals with higher defect densities could exhibit mesoporous structures, where the higher porosity allows for faster diffusion of gases for gas storage applications.31

To determine the extent of change in the ionic strength of the synthesis media caused by OmimCl addition, conductivity measurements were performed on synthesis mixtures without BDC and at 10% the Al(NO₃)₃ concentration used for hydrothermal synthesis (62.3 mM). Addition of various amounts of OmimCl caused an increase in conductivity between 0.36% and 17% compared to the control sample with only Al(NO₃)₃ (Table S3). This increase in conductivity with the addition of OmimCl is an insignificant increase considering the actual synthesis solutions contain 10 times the

concentration of $Al(NO_3)_3$ as well as dissolved BDC anions at high temperatures. Therefore, the increase in ionic strength caused by the addition of OmimCl is presumed to not be the primary driving force for accelerated crystallization along the [001] direction. Nevertheless, these conductivity measurements do not preclude the possibility of either Omim $^+$ or Cl $^-$ ions increasing the ionic strength in local microenvironments to promote crystal growth.

To attempt to elucidate the kinetics of MIL-53(AI) crystallization under the employed conditions, two experiments were performed, where MIL-53(AI) was grown in the absence or presence of 0.20% v/v OmimCl and reactions were quenched at 6, 12, 18, and 24 h time points. In the presence of 0.20% v/v OmimCl, both average particle size and rate of growth of particle size surpassed those of crystals synthesized without OmimCl. Using the ImageJ software to analyze particles sizes, an increase in particle size from 5.9 \pm 2.3 μ m to 6.6 \pm 2.0 µm from 6 h to 24 h, respectively, was observed in the presence of OmimCl, while these average particle sizes were 2.7 \pm 1.1 μm and $3.5 \pm 1.5 \,\mu m$ in the absence of OmimCl (Figs. 3a, S5). Moreover, after 6 h of reaction time, the morphology of the sample synthesized without OmimCl is dominated by small block-shaped particles, commensurate with the fact that particles are at the beginning of the growth stage (Fig. 3c). However, in the presence of OmimCl, longer rod-shaped crystals begin to form after 6 h of reaction time, demonstrating that OmimCl accelerates the self-assembly of MOF crystallites to form late-stage morphologies (Fig. 3d). Samples isolated at 12 h and 18 h follow the same trend (Fig. S6). XRD patterns also demonstrate accelerated crystallization caused by OmimCl, as evidenced by the relative crystallinity reaching 0.95 at 6 h compared to the 24 h sample (Fig. 3b), which was defined as 1.00. In comparison, the relative crystallinity was only 0.51 at 6 h and 0.79 at 24 h in the absence of OmimCl. By combining SEM and XRD results, we demonstrate that OmimCl indeed accelerates the rate of MIL-53(AI) crystal growth.

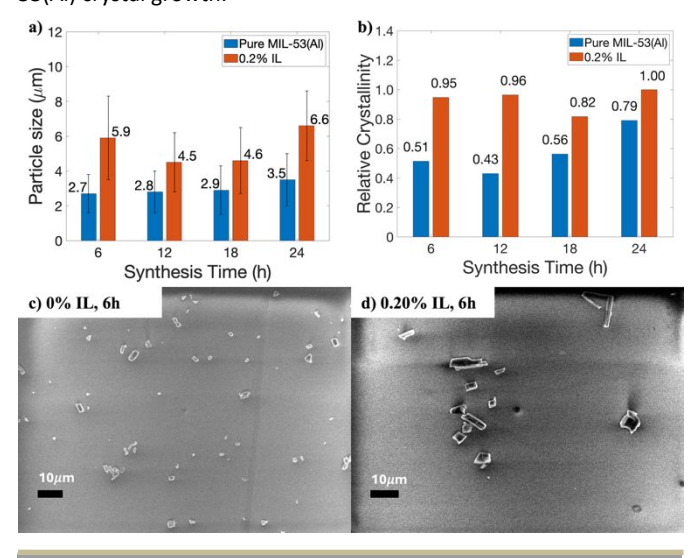


Figure 3. Evolution of particle size (a) and relative crystallinity (b) over time for pure MIL-53(AI) (blue) and MIL-53(AI) synthesized with 0.2% v/v OmimCI (orange). (c) SEM image of pure MIL-53(AI) isolated after 6 hours. (d) SEM image of MIL-53(AI) synthesized with 0.20% v/v OmimCI isolated after 6 hours.

COMMUNICATION PCCP

We propose a mechanism for the role of OmimCl in MIL(53)-Al crystal growth (Fig. 4) based on our results, which confirm that OmimCl promotes directional growth along the length of the MIL-53(AI) crystal at OmimCl volume fractions below 0.50%. Furthermore, the invariance of the crystallite size from XRD analysis suggests that individual crystallites are not affected by the IL and are instead preferentially aligned along the [001] direction to form larger crystal assemblies. In contrast, the synthesis without IL shows irregularly shaped crystals and agglomeration of crystallites, which is due to simultaneous nucleation and crystal growth.²⁶ These observations could be indicative of a nonclassical oriented attachment pathway32 or a mesocrystal-mediated fusing of crystallites.33 However, at IL concentrations above 0.50% v/v, decreases in relative crystallinity, particle size, and linker weight suggest arrested crystal growth accompanied by the introduction of defects. Surfactant micelles that introduce mesoscopic order have been reported for MOFs and our observations align with those made by Molina et al., making this a plausible explanation for the observed effects since OmimCl is known to form micelles. 16,34 Other sources of these effects exclusively at high IL concentrations could include Omim+ aggregation around MOF crystallites and hindered linker coordination due to excessive coordination of Cl⁻ ions to the Al secondary building units.35,36 Further work is required to confirm these complexes and intermediates. Even though all crystallizations were carried out at 200 °C, gathering information on how OmimCl affects MOF growth at this temperature could assist in developing strategies for reaction optimization at lower temperatures.

While our data strongly suggests preferential growth for samples prepared with up to 0.50% v/v OmimCl, inconsistencies in the data merit further experimentation. Most importantly, an explanation is lacking for why two crystallization outcome regimes are observed one above and another below 0.50% v/v OmimCl. Focusing experiments close to 0.50% v/v OmimCl could help elucidate why the crystallization outcome changes upon a critical IL concentration. These experiments should be complemented by density functional theory (DFT) calculations^{21,37} and molecular dynamics (MD) simulations^{38,39} investigating the nature of the interactions between OmimCl, linker, and metal ion. Two XRD peaks located at 11° and 22° in the diffraction patterns (Fig. 1a), which are especially pronounced in samples 1, 3, and 4, are not expected to be observed for MIL-53(AI)-np. These reflections could represent a foreign phase caused by strain from templating by the large Omim⁺ ions. The fact that the (110) peak is highly asymmetric (Fig. 1a inset) and that the relative intensities of the (200) and (111) peaks for pure MIL-53(Al)-np are much lower than predicted by XRD calculations, indicate possible microstrain-induced effects and asymmetric crystallite geometry, which require further analysis by 2D XRD methods (Table S1). To obtain a better picture of the crystallization kinetics of MIL-53(AI), additional samples are currently being synthesized and isolated at more frequent times. Further measurements are required to conclusively identify both the solution species responsible for MIL-53(Al) crystal elongation and higher crystallinities at low IL concentrations as well as the complexes that inhibit crystal growth at high IL concentrations.

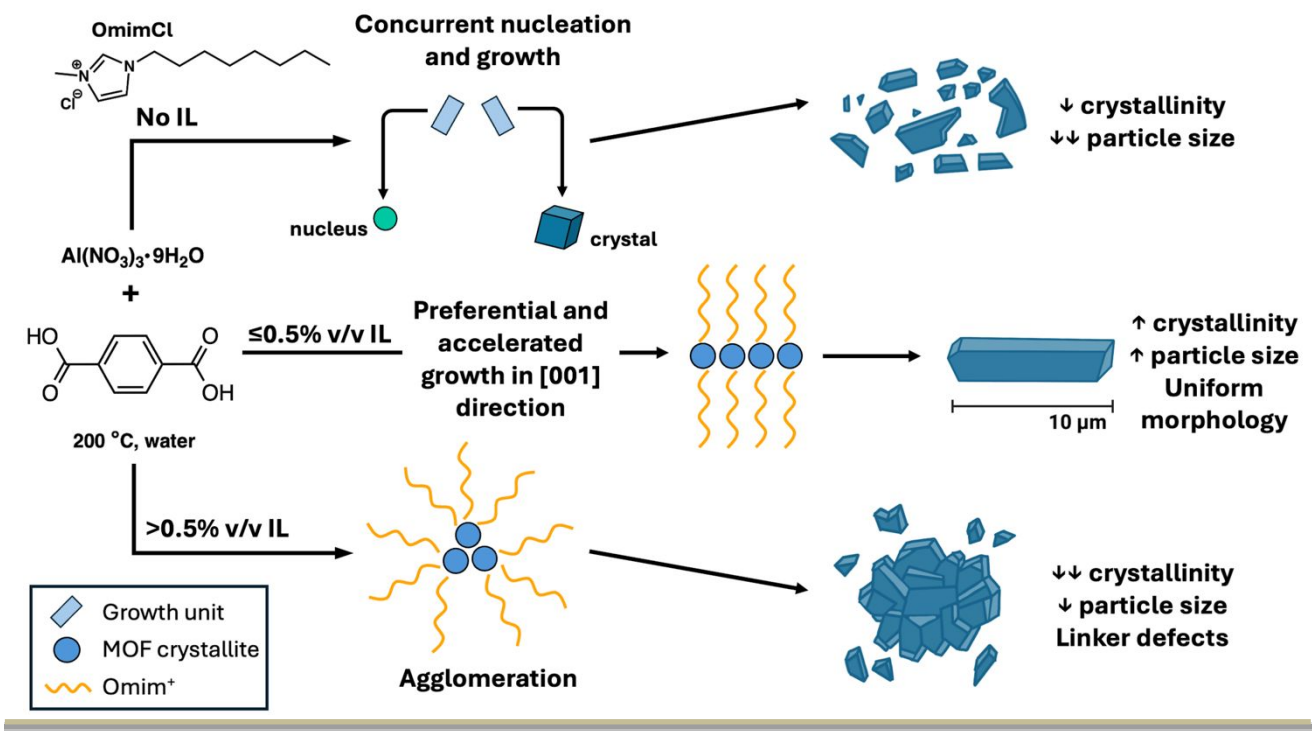


Figure 4. Proposed mechanism for the role of OmimCl in the crystallization of MIL-53(Al).

In conclusion, XRD and SEM results indicate that, with respect to the pure MIL-53(AI) sample, the addition of up to 0.50% v/v of the IL OmimCI to MIL-53(AI) hydrothermal synthesis solutions led to

increased crystallinity of up to 43% and larger particles through preferential growth along the [001] direction. At OmimCl concentrations above 0.50% v/v, decreases in relative crystallinity,

PCCP COMMUNICATION

particle size, regularity in particle morphology, and linker weight were observed. These results suggest that crystallite agglomeration and excess coordination by the Omim⁺ and Cl⁻ ions arrested crystal growth and generated defects. Quenching MIL-53(Al) crystallization in the presence of OmimCl at 6, 12, 18, and 24 h demonstrated an accelerated increase in crystallinity and particle size compared to crystallization in the absence of OmimCl. This work lays the groundwork for the optimization of reaction conditions at lower temperatures to reduce the energy cost of MOF synthesis. Continued research on the IL-directed preferential growth of MOFs shows promise towards achieving tuneable, predictive MOF syntheses. Current work focuses on elucidating how enhancements in MIL-53(Al) particle size and relative crystallinity by the addition of OmimCl impact MIL-53(Al) performance in the adsorption and photocatalytic degradation of organic dyes.

Conflicts of interest

There are no conflicts to declare.

Data availability

The data supporting this article have been included as part of the Supplementary Information.

Acknowledgements

The SEM facility at Bowdoin College was supported by NSF MRI grant no. 1590963. The NMR facility at Bowdoin College was financed by the William B. Beedle Life Sciences Fund, the Alan Irving Memorial Fund, and the Chemistry Development Fund. O.W. gratefully acknowledges the support received from the Bowdoin College Office of Student Fellowships and Research through a Bowdoin College Fall Research Award. P.S.V. gratefully acknowledges the support received from Bowdoin College through a Dana Walker Mayo Fund Fellowship. V.J. gratefully acknowledges the support received from Bowdoin College through a Kibbe Science Fellowship.

Notes and references

- 1 V. F. Yusuf, N. I. Malek and S. K. Kailasa, *ACS Omega*, 2022, **7**, 44507–44531.
- 2 T. U. Rehman, S. Agnello, F. M. Gelardi, M. M. Calvino, G. Lazzara, G. Buscarino and M. Cannas, *Nanomaterials*, 2024, **14**, 388.
- 3 C. W. Ashling, D. N. Johnstone, R. N. Widmer, J. Hou, S. M. Collins, A. F. Sapnik, A. M. Bumstead, P. A. Midgley, P. A. Chater, D. A. Keen and T. D. Bennett, *J. Am. Chem. Soc.*, 2019, **141**, 15641–15648.
- 4 S.-Y. Kim, J. H. Kang, S.-I. Kim and Y.-S. Bae, *Chemical Engineering Journal*, 2019, **365**, 242–248.

- 5 X. Chen, X. Liu, L. Zhu, X. Tao and X. Wang, *Chemosphere*, 2022, **291**, 133032.
- 6 O. Nahi, A. N. Kulak, A. Broad, Y. Xu, C. O'Shaughnessy, O. J. Cayre, S. J. Day, R. Darkins and F. C. Meldrum, *Crystal Growth and Design*.
- 7 K. Suresh, A. P. Kalenak, A. Sotuyo and A. J. Matzger, *Chemistry*, 2022, **28**, e202200334.
- 8 J. J. De Yoreo, P. U. P. A. Gilbert, N. A. J. M. Sommerdijk, R. L. Penn, S. Whitelam, D. Joester, H. Zhang, J. D. Rimer, A. Navrotsky, J. F. Banfield, A. F. Wallace, F. M. Michel, F. C. Meldrum, H. Cölfen and P. M. Dove, *Science*, 2015, **349**, aaa6760.
- 9 R. S. Forgan, *Chemical Science*, 2020, **11**, 4546–4562.
- 10 G. C. Shearer, S. Chavan, S. Bordiga, S. Svelle, U. Olsbye and K. P. Lillerud, *Chem. Mater.*, 2016, **28**, 3749–3761.
- 11 F. Wang, L. Zhu, Q. Wei and Y. Wang, *Royal Society Open Science*, 2020, **7**, 201212.
- 12 Y. Zhang, Y. Jia, M. Li and L. Hou, Sci Rep, 2018, 8, 9597.
- 13 J. Łuczak, M. Kroczewska, M. Baluk, J. Sowik, P. Mazierski and A. Zaleska-Medynska, *Advances in Colloid and Interface Science*, 2023, **314**, 102864.
- 14 J. Gao, M. He, Z. Yi Lee, W. Cao, W.-W. Xiong, Y. Li, R. Ganguly, T. Wu and Q. Zhang, *Dalton Transactions*, 2013, **42**, 11367–11370.
- 15 H.-S. Lu, L. Bai, W.-W. Xiong, P. Li, J. Ding, G. Zhang, T. Wu, Y. Zhao, J.-M. Lee, Y. Yang, B. Geng and Q. Zhang, *Inorg. Chem.*, 2014, **53**, 8529–8537.
- 16 M. A. Molina, N. R. Habib, I. Díaz and M. Sánchez-Sánchez, *Catalysis Today*, 2022, **394–396**, 117–124.
- 17 N. R. Habib, R. Sainz, A. M. Taddesse and I. Diaz, *Catalysis Today*, 2022, **390–391**, 316–325.
- 18 J. Liu, F. Zhang, X. Zou, G. Yu, N. Zhao, S. Fan and G. Zhu, *Chem. Commun.*, 2013, **49**, 7430–7432.
- 19 T. P. Vaid, S. P. Kelley and R. D. Rogers, *IUCrJ*, 2017, **4**, 380–392.
- 20 X. Sang, J. Zhang, J. Xiang, J. Cui, L. Zheng, J. Zhang, Z. Wu, Z. Li, G. Mo, Y. Xu, J. Song, C. Liu, X. Tan, T. Luo, B. Zhang and B. Han, *Nat Commun*, 2017, **8**, 175.
- 21 P. Zhang, X. Kang, L. Tao, L. Zheng, J. Xiang, R. Duan, J. Li, P. Chen, X. Xing, G. Mo, Z. Wu and B. Han, *CCS Chemistry*, 2023, **5**, 1462–1469.
- 22 F. Joly, P. Devaux, T. Loiseau, M. Arab, B. Morel and C. Volkringer, *Microporous and Mesoporous Materials*, 2019, **288**, 109564.

COMMUNICATION PCCP

- 23 R. Dutta, M. N. Rao and A. Kumar, Sci Rep, 2019, 9, 14741.
- 24 L. Xu, B. Liu, S.-X. Liu, H. Jiao, B. de Castro and L. Cunha-Silva, *CrystEngComm*, 2014, **16**, 10649–10657.
- 25 Z.-H. Zhang, L. Xu and H. Jiao, *Journal of Solid State Chemistry*, 2016, **238**, 217–222.
- 26 A. Taheri, E. G. Babakhani and J. Towfighi, *Adsorption Science & Technology*, 2018, **36**, 247–269.
- 27 J. M. Salazar, G. Weber, J. M. Simon, I. Bezverkhyy and J. P. Bellat, *The Journal of Chemical Physics*, 2015, **142**, 124702.
- 28 T. Li, N. Dang, W. Zhang, W. Liang and F. Yang, *Nanomaterials*, 2018, **8**, 991.
- 29 C. F. Holder and R. E. Schaak, ACS Nano, 2019, 13, 7359–7365.
- 30 I. Bezverkhyy, G. Ortiz, G. Chaplais, C. Marichal, G. Weber and J.-P. Bellat, *Microporous and Mesoporous Materials*, 2014, **183**, 156–161.
- 31 R. V. Listyarini, J. Gamper and T. S. Hofer, *J. Phys. Chem. B*, 2023, **127**, 9378–9389.
- 32 D. Li, M. H. Nielsen, J. R. I. Lee, C. Frandsen, J. F. Banfield and J. J. De Yoreo, *Science*, 2012, **336**, 1014–1018.
- 33 V. M. Yuwono, N. D. Burrows, J. A. Soltis and R. L. Penn, *J. Am. Chem. Soc.*, 2010, **132**, 2163–2165.
- 34 T. Singh and A. Kumar, J. Phys. Chem. B, 2007, 111, 7843-7851.
- 35 S. Liu, J. Liu, X. Hou, T. Xu, J. Tong, J. Zhang, B. Ye and B. Liu, *Langmuir*, 2018, **34**, 3654–3660.
- 36 V. Nozari, C. Calahoo, J. M. Tuffnell, D. A. Keen, T. D. Bennett and L. Wondraczek, *Nat Commun*, 2021, **12**, 5703.
- 37 G. Tian, W. Zhou, G. Tian and W. Zhou, in *Density Functional Theory Calculations*, IntechOpen, 2020.
- 38 S. M. Urahata and M. C. C. Ribeiro, *The Journal of Chemical Physics*, 2004, **120**, 1855–1863.
- 39 T. Frömbgen, J. N. Canongia Lopes, B. Kirchner and K. Shimizu, *J. Phys. Chem. B*, 2024, **128**, 3937–3945.

Bowdoin

Data Availability Statement

The data supporting this article have been included as part of the Supplementary Information.